Chemical Engineering Science 66 (2011) 2068–2079

Contents lists available at ScienceDirect

Chemical Engineering Science

journal homepage: www.elsevier.com/locate/ces

Droplet break-up by in-line Silverson rotor–stator mixer

S. Hall [a,*], M. Cooke [b], A. El-Hamouz [c], A.J. Kowalski [d]

[a] School of Chemical Engineering, University of Birmingham, Edgbaston, Birmingham, B15 2TT, UK
[b] School of Chemical Engineering & Analytical Science, The University of Manchester, Sackville Street, PO Box 88, Manchester, M60 1QD, UK
[c] Department of Chemical Engineering, An-Najah National University, Nablus, West Bank, PO Box 7, The Palestinian Authority, Occupied Palestinian Territory
[d] Unilever Research & Development, Port Sunlight Laboratory, Quarry Road East, Bebington, Wirral, CH63 3JW, UK

ARTICLE INFO

Article history:
Received 7 October 2010
Received in revised form
26 January 2011
Accepted 27 January 2011
Available online 2 February 2011

Keywords:
Emulsion
Emulsification
Energy dissipation rate
Rotor–stator mixer
Mixing
Scale-up

ABSTRACT

Silverson high shear in-line rotor–stator mixers are widely applied in industry for the manufacture of emulsion-based products but the current understanding of droplet breakage and coalescence in these devices is limited. The aim of this paper is to increase the understanding of droplet break-up mechanisms and to identify appropriate literature correlations for in-line rotor–stator mixers. Silicone oils with viscosities ranging from 9.4 to 969 mPa s were emulsified with surfactant in an in-line Silverson at rotor speeds up to 11,000 rpm and flow rates up to 5 tonnes/h. The effect of rotor speed, flow rate, dispersed phase fraction up to 50 wt%, inlet drop size and viscosity ratio on droplet size was investigated. It was found that rotor speed and dispersed phase viscosity have a significant effect on the droplet size, while flow rate, inlet droplet size, viscosity ratio and dispersed phase volume have a lesser effect. The results indicate that low viscosity droplets are broken by turbulent inertial stresses, while droplets smaller than the Kolmogorov length scale are broken by a combination of inertial and viscous stresses. It also appears that the weak dependence of drop size on flow rate enables the energy efficiency of an in-line high shear Silverson to be significantly improved by operating at as high a flow rate as possible.

1. Introduction

Emulsion manufacture by mixing two immiscible liquids is an important process operation in the production of a wide range of emulsion-based products, including shampoos, deodorants, salad dressings, medicines, bitumen and fertilisers (Thapar, 2004). Formulated structured products are highly dependent upon the manufacturing process and the chemical formulation, thus both the material and process parameters control the product properties.

One of the key pieces of process equipment widely employed in the manufacture of liquid–liquid dispersions is in-line high shear rotor–stator mixers, which have numerous industrial applications including blending miscible liquids, dispersing fine solid particulates into liquids and forming solid nanoparticle dispersions (Myers et al., 1999). Rotor–stator mixers are frequently used in process industries such as fine chemicals, food processing and pharmaceuticals (Maa and Hsu, 1996; Saadevandi and Zakin, 1996; Schubert, 1997; Atiemo-Obeng and Calabrese, 2004; Adler-Nissen et al., 2004) as they have the ability to achieve several process operations within a single unit operation, leading to increased process intensification. The main advantage of using these mixers is due to the creation of very high energy dissipation rates as the kinetic energy generated by the rotor is dissipated in the small stator volume, and high shear rates in the rotor–stator gap (Utomo et al., 2009).

Despite the extensive industrial application of rotor–stator devices, little emphasis has been placed on understanding the processing principles, which is summarised by Atiemo-Obeng and Calabrese (2004)

> *"The current understanding of rotor–stator devices has almost no fundamental basis. There are few theories by which to predict, or systematic experimental protocols by which to assess, the performance of these mixers. In fact there are few archival publications on rotor–stator processing".*

Moreover, knowledge relating to emulsification by in-line rotor–stator devices is further limited. At present, process development of emulsion-based products is based on trial and error, which results in higher development costs, start-up problems, lost time to market and considerable material waste due to the numerous trials required from laboratory scale to plant scale (Calabrese et al., 2000).

The key parameter often used to describe how process and physical properties affect emulsification is the surface area weighted mean droplet diameter, $d_{3,2}$, also known as the Sauter mean diameter. Sauter mean diameter, defined as a ratio of the

* Corresponding author.
E-mail address: stevenhall28@yahoo.co.uk (S. Hall).

0009-2509/$ - see front matter © 2011 Elsevier Ltd. All rights reserved.
doi:10.1016/j.ces.2011.01.054

third and second moments of a drop size distribution, preserves both the total volume of the dispersed phase and total interfacial area of the population of drops, and is commonly used to characterise droplet size distributions for drop size reduction processes since it is inversely proportional to the total dispersed phase surface area (Leng and Calabrese, 2004).

Expressions for correlating Sauter mean diameter have been reported by many authors for a range of formulations and processing equipment, with most of the previous work summarised by Leng and Calabrese (2004). Models developed by Hinze (1955) have often been used as the basis to develop a mechanistic understanding of droplet breakage (Leng and Calabrese, 2004). These models apply the concept of a cascade of turbulent eddies of varying sizes, developed by Kolmogorov, which assumes homogenous isotropic turbulence, and whilst this assumption in rarely correct in practise, the theory has nevertheless proved useful and instructive. This approach divides the mechanisms of droplet breakage on the basis of whether the drop size is greater or smaller than the Kolmogorov length scale (η_K), which defines the boundary between the point where the inertial and viscous stresses acting on the drop are equal. Rotor–stator mixers can produce drops in the order of η_K or smaller (Calabrese et al., 2000), where interactions within the viscous subrange become important and viscous forces are critical. As a result, it is difficult to clearly identify the breakage mechanisms and whether they occur simultaneously or in sequence.

For drop sizes larger than η_K, for dilute low viscosity dispersed phase liquid–liquid systems, the drops are inviscid and the interfacial tension surface force contributes to stability. The maximum stable equilibrium drop size can be related to the energy dissipation rate (based on the swept rotor volume) by the following general relationship (Leng and Calabrese, 2004):

$$d_{3,2} \approx \left(\frac{\sigma}{\rho_c}\right)^{3/5} \varepsilon^{-2/5} \tag{1}$$

Shinnar (1961) suggests that for drop sizes smaller than η_K, where the applied stress on the drop is inertial, that the following equation may be applied

$$d_{3,2} \approx \sigma^{1/3} \rho_c^{-2/3} \mu_c^{1/3} \varepsilon^{-1/3} \tag{2}$$

For drops smaller than η_K, where viscous stresses on the drop are important for droplet breakage, Shinnar (1961) suggests

$$d_{3,2} \approx \sigma^{1} \rho_c^{-1/2} \mu_c^{-1/2} \varepsilon^{-1/2} \tag{3}$$

For drop sizes larger than η_K, for high viscosity dispersed phase systems, viscous stresses become more important than surface forces for resisting droplet deformation and the following expression is obtained (Leng and Calabrese, 2004)

$$d_{3,2} \approx (\rho_c \rho_d)^{-3/8} \mu_d^{3/4} \varepsilon^{-1/4} \tag{4}$$

The effect of viscous stresses due to the viscosity of the dispersed phase on drop size is covered by two approaches in literature for stirred vessels, which may be appropriate for high shear mixers. Calabrese et al. (1986) developed Eq. (4), which, for geometrically similar systems with a constant power number (Po), can be simplified by introducing the dimensionless Weber number and viscosity group

$$\frac{d_{3,2}}{D} = C_1 We^{-3/5} \left[1 + C_2 Vi \left(\frac{d_{32}}{D}\right)^{1/3}\right]^{3/5} \tag{5}$$

In the second approach, Davies (1985) included a viscosity resistance term divided by the break-up time, to Eq. (1) to obtain

$$d_{3,2} = C_3 \sigma^{3/5} \left(1 + \frac{C_4 \mu_d (\varepsilon . d_{3,2})^{1/3}}{\sigma}\right)^{3/5} \rho_c{}^{-3/5} \varepsilon^{-2/5} \tag{6}$$

In literature for stirred vessels, the effect of dispersed phase volume on drop size has typically been correlated for inviscid drops in clean systems according to (Leng and Calabrese, 2004)

$$\frac{d_{3,2}}{D} = C_5 (1 + C_6 \Phi) We^{-3/5} \tag{7}$$

The constant C_5 is geometry dependent, while of C_6 is a measure of the tendency of the system to coalesce and can range from 3 to 20 for clean systems (Pacek et al., 1999).

Drop size correlations can either be based on theoretical mechanistic models discussed above or alternatively on empirical equations, described below. To evaluate the droplet disruption efficiency for continuous emulsification processes, Karbstein and Schubert (1995) proposed volumetric specific energy or energy density, E_V

$$d_{3,2} \approx E_V{}^{b} \approx \left(\frac{P}{Q}\right)^{b} \tag{8}$$

Energy density describes the effect of process parameters applied to a certain emulsion volume and accounts for the mean residence time acting on the drop assuming no recoalescence. Karbstein and Schubert (1995) stated that if b is in the order of -0.4, turbulence is important for droplet disruption and Schubert and Engel (2004) summarised exponents for rotor–stator mills of ~ -0.35 for turbulent inertial forces and ~ -0.75 for turbulent shear forces.

The majority of work relating to liquid–liquid dispersion in rotor–stator mixers is based on batch systems. Davies (1985) investigated the emulsification of immiscible liquids in colloid mills and found that the turbulent fluctuating velocity is important for drop breakage. Calabrese et al. (2000) investigated a batch Ross rotor–stator mixer and found little effect of volume fraction, stator geometry and interfacial tension on drop size for a dilute system. Based on the value of the exponent on energy dissipation rate they concluded that droplet interaction with inertial subrange eddies and sub-Kolmogorov scale viscous stresses are important for droplet breakage. Similar conclusions were confirmed by Padron (2005) who furthered this work by studying liquid–liquid systems stabilised by surfactants in a batch Silverson mixer.

Adler-Nissen et al. (2004) examined a lab scale rotor–stator to produce small volumes of high phase volume emulsions, similar to mayonnaise. This work varied the rotor speed to investigate the effect of shear stress on droplet size. Khopkar et al. (2009) studied formulation parameters for a batch impeller and rotor–stator device, and found that viscosity ratio did not impact on the median droplet size, but the effect of dispersed phase content was more significant for a surfactant stabilised emulsion system.

In-line rotor–stator studies on emulsification are scarce but include work by Averbukh et al. (1988) and more recently by Thapar (2004) and Gingras et al. (2005). Averbukh et al. (1988) provides an expression correlating drop size with various terms such as dispersed phase volume fraction, interfacial tension, flow rate, shear gap, continuous phase viscosity and rotor speed; however, a description of this study is not clear.

Thapar (2004) investigated the effect of stator geometry, rotor speed and flow rate, and dispersed phase volume fraction on mean drop size in a Silverson mixer; however, only two flow rates and one formulation were investigated. He found that rotor speed and dispersed phase volume fraction had the strongest effect on Sauter mean diameter.

Gingras et al. (2005) carried out bitumen emulsification using a continuous pilot plant scale Silverson rotor–stator mixer. The process parameters investigated include rotor speed, flow rate, temperature (30–90 °C) and dispersed phase content

(55–75 wt%). They found that droplet size decreases as rotor speed increases, or as temperature of the bitumen dispersed phase fraction decreases. Their results did not follow any of the models tested and they suggested that this was due to high recoalescence rates between very viscous drops at high viscosity ratios.

Kevala et al. (2005) analysed drop size distributions in a single pass in-line rotor–stator mixer by injecting oil directly into the mixing head. For low viscosity dispersed phases the drop size distribution was found to be bimodal, becoming single modal at the highest rotor speeds and the lowest flow rates. For high viscosity dispersed phases the drop size distribution was single modal, and became more bimodal when rotor speed was increased, and flow rate decreased.

Literature on emulsification using in-line rotor–stator mixers is limited; hence, this study aims to increase the present understanding of emulsification in these devices and examine possible literature correlations and droplet breakage mechanisms. This work investigates process parameters and formulation variables such as dispersed phase content, dispersed phase viscosity and viscosity ratio on the drop size distributions (DSDs). Droplet size data is correlated with commonly used parameters including energy density and energy dissipation rate to gain a fundamental understanding to allow results obtained for one formulation to be applied to other systems.

2. Materials and Methods

2.1. Equipment

The experimental rig (Fig. 1) consists of an agitated mixing vessel to prepare the emulsions and an in-line Silverson high shear rotor–stator mixer (Silverson Machines Ltd., Chesham, UK). The Silverson rotor–stator mixer is a pilot plant scale 150/250 MS model, containing double concentric rotors, which sit within standard double emulsor screens, shown in Fig. 2. The mixer is driven by a 22 kW motor controlled by a frequency inverter and may be run to a maximum rotor speed of 12,000 rpm. The rotor–stator gap is 0.24 mm, and the main details and dimensions of the Silverson mixer rotor–stator geometry are given in Table 1.

The coarse emulsions were prepared in two mixing vessels of 60 and 800 L capacity, but for simplicity only one is shown in Fig. 1. The 800 L mixing vessel is fitted with a 0.31 m diameter Cowles Disc type impeller while the 60 L vessel contains a 0.13 m diameter high shear dissolver disc similar to the Cowles Disc. The coarse emulsions were prepared by controlling both the impeller speed in the mixing vessels and the mixing time to achieve the desired inlet drop size to the Silverson, which ranged from ~20 to 70 μm. The 800 L vessel was used for low phase fraction oil emulsions (1–5 wt%) and allowed high flow rates up to 1.33 kg/s to be investigated. For higher phase volume emulsions (> 5 wt%), the amount of oil required was prohibitive and only 60 L batches were made, with the flow rate limited to 0.83 kg/s.

Coarse emulsions from the smaller vessel were pumped via a 38.1 mm pipeline to the rotor–stator mixer with a rotary tri-lobe

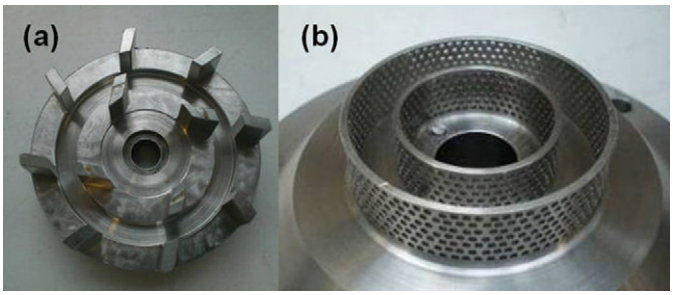

Fig. 2. Image of (a) standard double rotors and (b) standard double emulsor screens for the Silverson 150/250 MS rotor–stator mixer.

Table 1
Main details and dimensions of the Silverson rotor–stator mixer geometry.

	External diameter (mm)	Internal diameter (mm)	Details
Inner rotor	38.1	–	4 blades
Outer rotor	63.5	–	8 blades
Inner screen	42.3	38.6	6 rows of 50 × 1.59 mm circular holes on a 2.54 mm triangular pitch, 300 holes
Outer screen	67.7	64.0	7 rows of 80 × 1.59 mm circular holes on a 2.54 mm triangular pitch, 560 holes

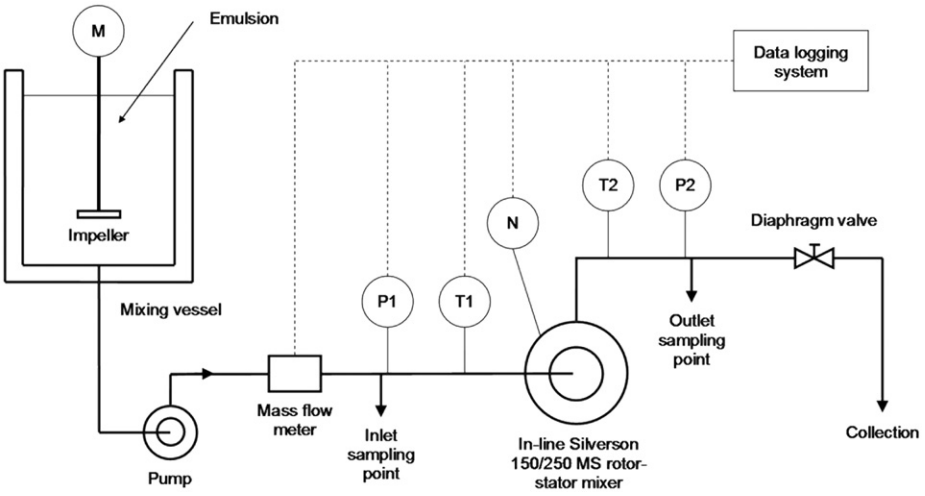

Fig. 1. Schematic diagram of the Silverson rotor–stator experimental arrangement.

pump, while a centrifugal pump was used for emulsions from the larger vessel. The inlet pipeline incorporates a Coriolis mass flow meter, while both the inlet and outlet pressures and temperatures were measured.

2.2. Materials

Oil-in-water emulsions with silicone oil (poly-dimethyl siloxane, Dow Corning 200 fluid) as the dispersed phase and water as the continuous phase were investigated. All emulsions contained a 0.5% concentration by weight of sodium laureth sulphate (SLES) surfactant (SLES 2EO, 'Texapon N701', Cognis UK Ltd., Hertfordshire). The SLES surfactant was a commercial grade supplied as a 70 wt% active viscous yellow liquid.

Silicone oil viscosities ranging from 9.4 to 969 mPa s (Table 2) were examined at phase fractions of 1, 5, 25 and 50 wt% of the total emulsion batch. Viscosity ratio was varied by adding sodium carboxyl methyl cellulose (CMC), (Hercules powder, grade 7H4C), to thicken the continuous phase. As CMC solutions are shear thinning, the characteristic shear rate was calculated in order to determine the apparent continuous phase viscosities. CMC concentrations of 0.05%, 0.15%, 0.4% and 0.8% by weight of the aqueous phase for oil viscosities of 9.4–339 mPa s (Table 3), were chosen to achieve a range of viscosity ratios from 0.46 to 381 at the highest rotor speed of 11,000 rpm.

The interfacial tensions between the oils and the surfactant solutions (Table 2) were measured using the pendant drop method. In this method interfacial tension is calculated from the balance between the gravity force and surface forces at the moment of drop separation from the nozzle (Davies and Rideal, 1961).

The apparent viscosity of the aqueous CMC continuous phases at 25 °C (Table 3) were measured using a Haake RV20 viscometer fitted with either an MV1 or MV2 rotor, depending on the viscosity. The shear profile was increased over the range from 2 to 450 s^{-1}, before decreasing again over the same range. The CMC solutions are shear thinning and follow the power-law viscosity relationship.

Table 2
Silicone oil properties at 25 °C.

Silicone oil viscosity, μ_d (mPa s)	Density, ρ_d (kg/m^3)	Interfacial tension with 0.5 wt% SLES solution, σ (mN/m)	
		0 wt% CMC	0.8 wt% CMC
9.4	937	10.6	8.9
48	957	12.7	10.9
97	965	11.9	10.4
339	969	12.3	10.9
969	969	12.7	10.8

2.3. Emulsion preparation

SLES was added to the vessel filled with water at 25 °C, and allowed to completely dissolve to create a well-mixed solution. The amount of surfactant required for full surface coverage of the oil droplets is estimated to be 1.2 mg/m^2, calculated assuming that all the drops are of the same diameter (Sauter mean diameter), and are completely covered by surfactant with a head group size of the order of 0.6 nm^2 per molecule (Goloub and Pugh, 2003). The concentration of surfactant used in all experiments of 5000 ppm was in excess to ensure full surface coverage and long-term emulsion stability (El-Hamouz, 2007). The quantity of surfactant required to cover the smallest drops for a 50 wt% dispersed phase fraction emulsion in this study represents ~13% of the total available surfactant.

Silicone oil was then added to the tank surface, but for the CMC solutions bulk mixing was slower and the oil was injected directly into the impeller region. Adding the oil to the impeller region allows the target size distribution to be obtained sooner (El-Hamouz et al., 2009). Once the target drop size in the range 20–70 μm was achieved, the vessel impeller speed was reduced to a lower agitation speed to maintain a well-mixed dispersion and prevent creaming during the experiment.

2.4. Emulsification procedure

The coarse emulsion was fed to the Silverson mixer in a single pass at a series of flow rates and rotor speeds to investigate droplet size reduction. For the dilute emulsions (1–5 wt%), samples were taken at rotor speeds from 3000–11,000 rpm at a constant flow rate of 300 kg/h; and then at a constant speed of 11,000 rpm for flow rates between 300–4800 kg/h. For the concentrated emulsions (> 5 wt%), samples were only taken at rotor speeds of 3000–11,000 rpm at a constant flow rate of 300 kg/h.

Flow rate was controlled by a diaphragm valve downstream of the mixer (Fig. 1). A pump was used to maintain a slightly positive pressure on the inlet of the Silverson mixer, although it was not possible to maintain positive pressure at very high flow rates (> 2400 kg/h). The drop size distributions measured in the holding tank and at the inlet of the Silverson after passing through the pump were identical. At steady state flow rates and temperatures, a sample was taken from the sampling points at the inlet and the outlet of the Silverson.

2.5. Droplet size analysis

A Mastersizer X long bed laser diffraction particle analyser (Malvern Instruments, Malvern, UK) was used to measure the drop size distributions. A lens of focal length 300 mm was employed as this provided the most suitable range of drop size measurement of 1.2–600 μm. Samples were diluted in water/SLES solution to ensure the oil droplets were dispersed in a medium

Table 3
Typical rheological properties of the CMC continuous phases investigated at 25 °C.

CMC concentration (wt%)	Power law index, n	Constant, k (Pa s)^n	Apparent continuous phase viscosity, η (mPa s)		Kolmogorov length scale, η_K (μm)	
			3000 rpm	11,000 rpm	3000 rpm	11,000 rpm
0	–	–	0.89	0.89	5.2	2.0
0.05	0.0146	0.7971	3.03	2.33	13.1	4.2
0.15	0.0483	0.7648	7.12	5.75	26.6	8.3
0.40	0.4614	0.5970	20.34	12.05	54.2	13.5
0.80	3.2191	0.4605	42.63	24.46	94.9	21.4

similar to the continuous phase, and to prevent coalescence and oil deposition on the optical windows of the sample cell. The relative refractive indices (RI) used were 1.33 for the continuous water phase, and 1.42 for the silicone oil dispersed phase. The imaginary component of the absorption index for silicone oil was taken as 0.001. Emulsion samples measured directly after production were found not to change over 48 h, and produced similar distributions after many months, due to the presence of excess anionic SLES surfactant. For consistency, samples were measured within 48 h after the experiment was completed.

3. Results and discussion

3.1. The effect of inlet droplet size on outlet droplet size

The coarse emulsions prepared in the batch stirred vessels will inevitably show a degree of variation in droplet size over the experiments so the effect of the inlet drop size (Sauter mean diameter) on the outlet drop size from the Silverson mixer was investigated. Outlet drop size for 1–50 wt% 339 mPa s silicone oil emulsions as a function of impeller speed (N) for a range of inlet drop sizes from 23 to 62 μm are shown in Fig. 3. As expected, the outlet Sauter mean diameter is inversely related to the rotor speed, but there does not appear to be any systematic trends between the outlet and the inlet droplet sizes. A single power law relationship fit to all of the data in Fig. 3 gives a regression value, R^2 of 0.931. Therefore, it seems that the Silverson emulsification performance does not strongly depend on variations in the inlet drop size that may arise from upstream process unit operations. This result suggests that outlet drop size is dependant mainly on the operating conditions of the Silverson, possibly due to a combination of very high shear rates and the containing effect of the stator which helps to concentrate the flow.

3.2. The effect of rotor speed on droplet size

Fig. 4 shows the effect of rotor speed on drop size for 1 wt% silicone oil emulsions at a flow rate of 300 kg/h for all the viscosities studied. These results indicate that rotor speed has a strong effect on the emulsion drop size, with Sauter mean drop diameter proportional to N^b, where $b=-1.14$ to -1.29 for all viscosities except the most viscous oil where $b=-0.86$. The models in Eqs. (1)–(3) are based on energy dissipation rate, which is proportional power draw,

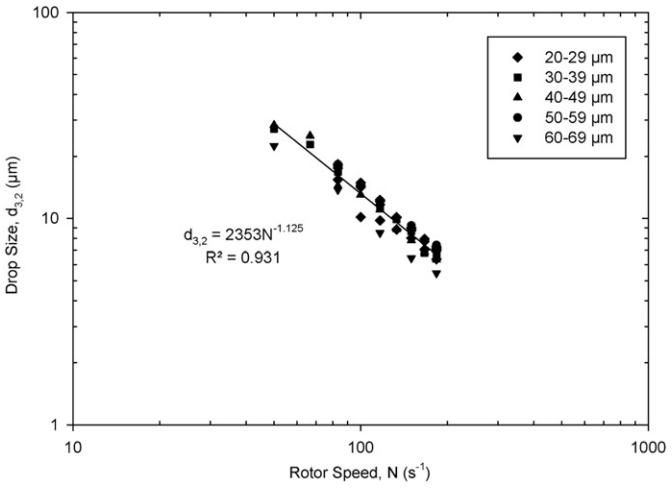

Fig. 3. Effect of rotor speed on drop size for a range of inlet drop sizes. Flow rate is 300 kg/h and dispersed phase viscosity is 339 mPa · s.

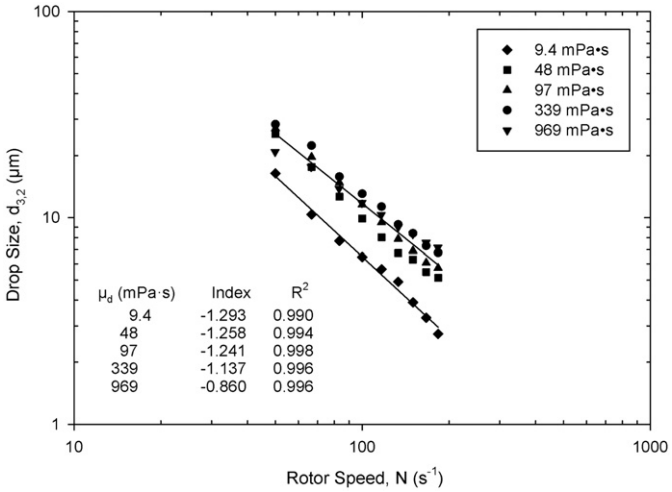

Fig. 4. Effect of rotor speed on drop size for a range of dispersed phase viscosities for a flow rate of 300 kg/h and dispersed phase fraction of 1 wt.%. The inlet drop sizes range from 28 to 54 μm.

which for a fixed low flow rate is approximately proportional to N^3. For turbulent inertial break-up, b should equal -1.2 for drop sizes larger than η_K, while for drops below the Kolmogorov length scale, Shinnar (1961) suggested $b=-1$. For drop sizes smaller than η_K when viscous stresses are important for breakage, b should equal -1.5 (Shinnar, 1961). The results from this investigation cover a range of exponents; however, turbulent inertial break-up is more likely since the majority of the drops are above the Kolmogorov length scale, calculated to be of the order of 2–5 μm, which is only comparable to the size of the smallest drops produced (Table 3). Applying the Kolmogorov theory to this data suggests that drop breakage is due to turbulent inertial stresses with a transition in breakage mechanism when the viscous stresses are great at the highest viscosity oil. For viscous dispersed phases, b should equal -0.75 when viscous forces are important for stabilising the drop (Leng and Calabrese, 2004), and b reduces to -0.86 for the highest viscosity oil. However the models in Eqs. (1)–(3) are for inviscid drops when the effect of dispersed phase viscosity is negligible, but Fig. 4 shows that there is a viscosity effect over the range 9.4–339 mPa s, when b is > -1.14. This discrepancy may be due in part to the fact that the assumption of homogenous isotropic turbulence is unlikely to be true inside the mixing head, and rotor–stator mixers have complex flow regimes, which will be discussed further in Section 3.5. Furthermore, the flow in the Silverson is highly irregular with regions of high energy dissipation rate near the rotor and regions where turbulent flow may not fully develop at short residence times; hence, simple shear flow may be important.

Arai et al. (1977) found for emulsions of polystyrene-o-xylene in aqueous polyvinyl alcohol solutions dispersed using a disc turbine agitated system, that the higher viscosity data (>520 mPa s) fitted closer to a slope of -0.75, while the lower viscosities (<34 mPa s) fitted more appropriately to a -1.2 gradient. This is seemingly because the drop size was larger than the Kolmogorov length scale. This observed trend is similar to the results of this work where a lower gradient of -0.86 is found for the highest viscosity of 969 mPa s.

The plot in Fig. 4 also shows a marked difference between the drop sizes for the 9.4 mPa s oil viscosity and the higher oil viscosities (48–969 mPa s), where the 9.4 mPa s experiments consistently produce smaller droplets over a range of rotor speeds. In Fig. 5 the volume DSD as function of rotor speed for the 9.4, 97 and 969 mPa s silicone oil emulsions is given. The

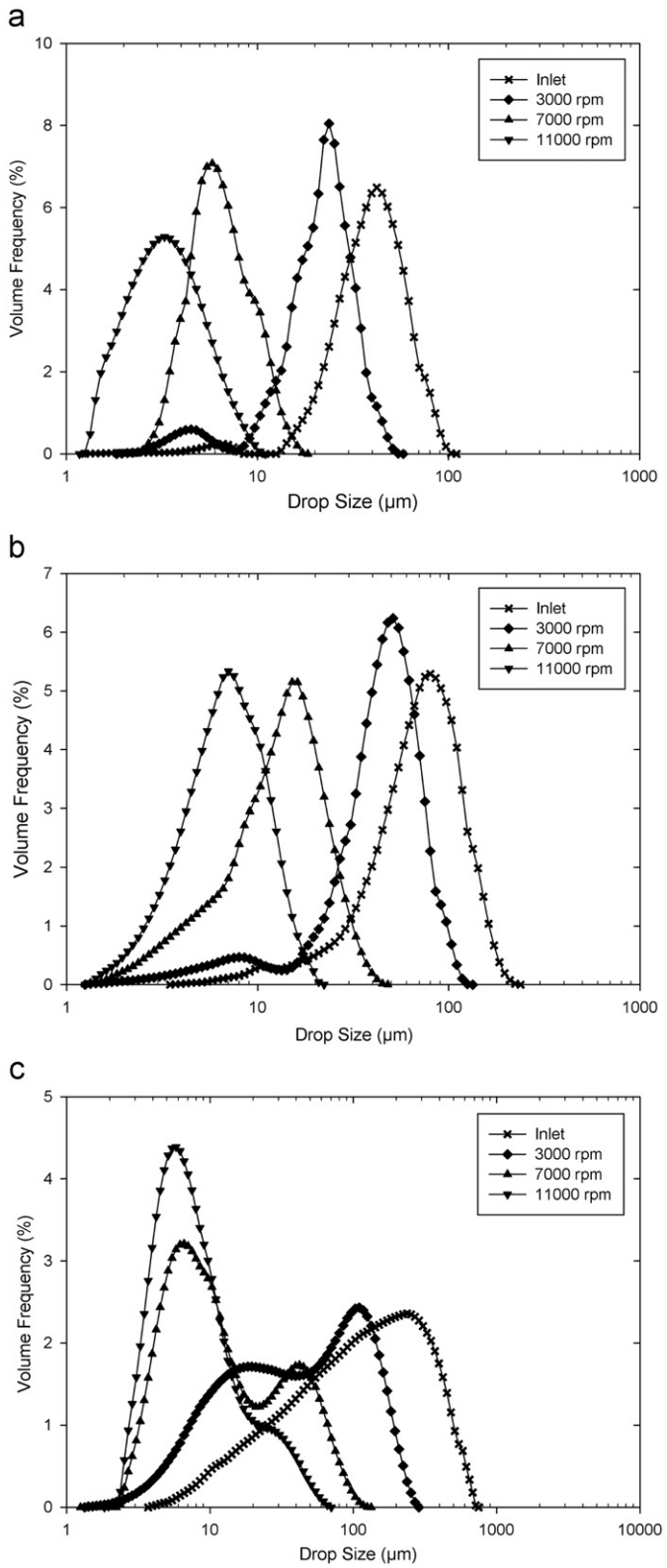

Fig. 5. Effect of rotor speed on the volume drop size distribution for 1 wt.% emulsion of (a) 9.4 mPa · s, (b) 97 mPa · s and (c) 969 mPa · s silicone oils at a flow rate of 300 kg/h.

distributions for the two lower viscosity oils are all predominantly monomodal and the whole size distribution shifts to smaller droplet sizes with increasing rotor speed. This trend in drop size reduction is consistent with the findings of Calabrese et al. (2000), Padron (2005) and Thapar (2004) for rotor–stator devices.

The DSD for the 969 mPa s silicone oil emulsion is greatly different to the other viscosities as all the rotor speeds show a pronounced bimodal distribution with the emergence of a peak at smaller drop sizes (<20 μm) at the expense of a peak at a larger drop size. However both the smaller and larger drop size peaks shift to a smaller drop size as observed for the lower viscosity oils. The formation of a bimodal distribution for high viscosities at higher rotor speeds was observed by Kevala et al. (2005) for a rotor–stator mixer.

Theoretical models of droplet breakage assume an equilibrium Sauter mean diameter has been achieved, which is not the case for the data presented in this paper as the drop sizes are for a single pass through the mixer. However theoretical models have only been applied to drop sizes produced at a constant flow rate; thus, the mean time drops are exposed to shear forces is the same. Single pass emulsification is the focus of this work as this experimental arrangement easily allows many processing conditions to be examined, and single pass processing is important for many industrial processes. Multiple pass emulsification is beyond the scope of this paper but will be examined in a further study.

3.3. The effect of flow rate on droplet size

Fig. 6 presents the plot of drop size as a function of flow rate for two rotor speeds of 11,000 rpm and for selected viscosities at 6000 rpm. In general droplet size is found to be almost independent of flow rate. At 6000 rpm, the three dispersed phase viscosities examined show that droplet size is almost identical for a range of flow rates, and there is little flow rate dependency. At 11,000 rpm the drop sizes are of course smaller, but there appears to be a slight dependence on flow rate for the lower flow rates, which is extremely weak. This may suggest that the role of the stator becomes increasingly important for droplet breakage as flow rate is increased, as the velocity and pressure drop through the stator increases. Fig. 7, the DSD for the 97 mPa s silicone oil, illustrates the small effect of flow rate on the whole volume distribution.

The 9.4 mPa s oil is an exception where there appears to be a fairly strong relationship between drop size and flow rate with a power law index of 0.19 and $R^2=0.923$. A possible reason for this observation could be as a result of a change in breakage mechanism as observed in the DSDs in Fig. 5. The formation of a small

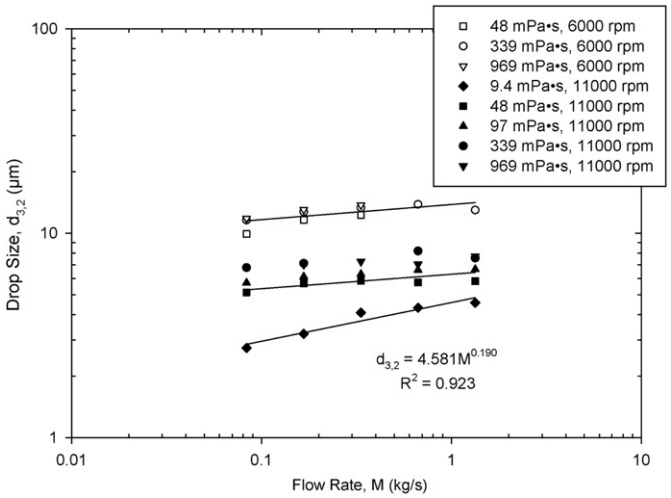

Fig. 6. Effect of flow rate on drop size for two rotor speeds of 6000 rpm and 11,000 rpm for a range of dispersed phase viscosities at a dispersed phase fraction of 1 wt.%.

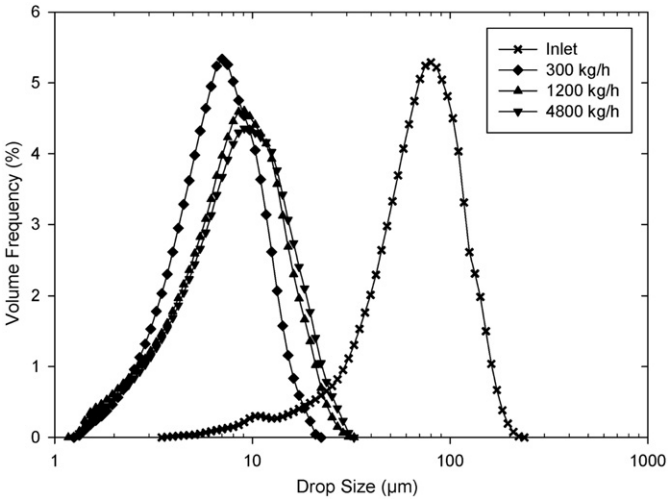

Fig. 7. Effect of flow rate on the volume drop size distribution for 1 wt.% 97 mPa · s silicone oil emulsion for a flow rate of 300 kg/h.

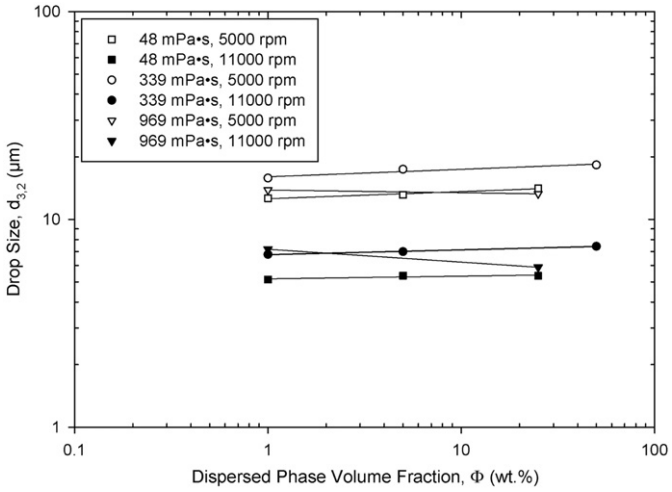

Fig. 8. Effect of dispersed phase volume fraction on drop size for a range of dispersed phase viscosities at rotor speeds of 5000 rpm and 11,000 rpm for a flow rate of 300 kg/h. The inlet drop sizes range from 29 to 48 μm.

peak of daughter drops at smaller droplet sizes for higher oil viscosities, suggests that droplet breakage is more dependent upon extensional flow than simple shear flow as dispersed phase viscosity increases (Padron, 2005). Larger high viscosity drops are easier to deform but once they are broken down to a critical droplet size, the droplet deformation time of the smaller drops seemingly exceeds the residence time in the high shear regions and further breakage cannot occur for all flow rates and drop size remains roughly independent of flow rate. Low viscosity droplets have a shorter deformation time and have a lower viscosity ratio, hence can be broken to a greater extent by simple shear flow; thus, lower viscosity drops are broken further by an increase in residence time. The effect of dispersed phase viscosity will be discussed further in Section 3.5.

At the highest flow rate examined of 4800 kg/h (1.33 kg/s), for all oil viscosities it is observed that drop size begins to fall slightly. To achieve these flow rates the centrifugal pumps were required, which did not affect the inlet drop size to any significant degree but is likely to cause cavitation. Despite the pressure head created by the pump, the inlet pressure to the Silverson was very negative (-0.9 bar), which was found to reduce the outlet drop size by ~ 0.5 μm at the highest rotor speed studied, at a constant flow rate.

For a rotor–stator mixer using bitumen emulsions, Gingras et al. (2005) also found no clear effect of flow rate. Ludwig et al. (1997) found the drop size to be slightly higher for higher flow rates, while Thapar (2004) obtained smaller drop sizes at higher flow rates; however, both effects were diminished at higher rotor speeds. Thapar (2004) found differences in $d_{3,2}$ of 10–15 μm at a tip speed of $\sim$10 m/s, and Ludwig et al. (1997) observed changes in $d_{4,3}$ of 2–3 μm for a tip speed of 4.1 m/s in a screw loop reactor.

3.4. The effect of dispersed phase volume fraction on droplet size

Fig. 8 shows that the impact of the dispersed phase volume fraction on the droplet size is not significant up to $\sim$50%. At both rotor speeds of 5000 and 11,000 rpm there appears to be no trend with oil viscosity. These results are expected as the presence of excess surfactant aids the prevention of coalescence as phase volume is increased. These findings are consistent with much of the literature, which finds either no or a weak relationship of drop size with phase volume for non-coalescing systems. However it can be observed that at 11,000 rpm, the drop size at 969 mPa s begins to decrease as phase volume increases, which supports the possibility of the beginning of droplet breakage where viscous stresses dominate as the emulsion viscosity increases. Vankova, et al. (2007) studied Φ up to 80% within a narrow-gap homogeniser, and confirmed a sharp decrease in $d_{3,2}$ for $\Phi > 50\%$, which was more pronounced for highly viscous oils. The authors proposed that the emulsification regime changed from turbulent inertial to turbulent viscous at very high volume fractions resulting in a reduction in droplet size.

To correlate Sauter mean diameter with dispersed phase volume fraction, a modified version of Eq. (1) is often used for inviscid drops (Leng and Calabrese, 2004). Oil viscosities of 48–969 mPa s fit the correlation in Eq. (7) with a regression coefficient, $R^2 = 0.964$

$$\frac{d_{3,2}}{D} = 0.250(1 + 0.459\Phi)We^{-0.58} \tag{9}$$

The low value of the C_6 (0.46) indicates that coalescence is minimal. Thapar (2004) found droplet size to decrease with a reduction of dispersed phase content. However, Thapar suggested this was not due to coalescence but was a result of the oil being injected into the continuous phase upstream of the Silverson mixer. He suggested that at higher Φ, the injection method may cause the oil phase to be harder to disperse in the inlet pipeline and result in large globules of oil bypassing the mixing head and not being well dispersed. For a batch mixer, Calabrese et al. (2000) found droplet size to be independent of phase volume for a range of Φ, from 0.08 to 0.24% by volume.

Khopkar et al. (2009) varied phase volume from 10% to 50% in a rotor–stator mixer inserted into a batch vessel using 60 mPa s oil. They found drop size to increase as phase volume increased, and the DSDs to become wider and bimodal. The results in this study indicate that the $d_{3,2}$ and DSDs remain relatively constant for a range of dispersed phase volumes, and bimodality does not develop as Φ increases. Fig. 9 presents the DSD for 339 mPa s silicone oil emulsion at phase volumes up to 50 wt%, and indicates that bimodality does not develop and the distribution width remains practically the same. Fig. 9 also shows that increasing phase volume reduces the fraction of drop sizes < 5 μm, possibly due to coalescence of the very smallest drops.

For a screw loop reactor, Ludwig et al. (1997) found higher drop sizes for an increase in volume fraction, up to 50%. However, at the highest rotational speed investigated corresponding to a tip

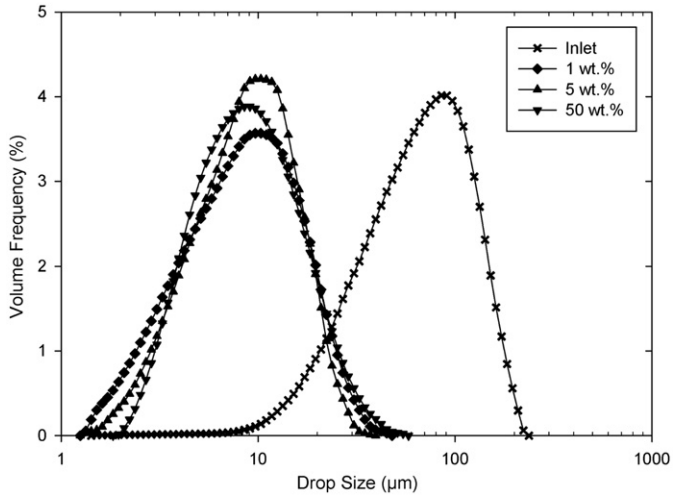

Fig. 9. Effect of dispersed phase volume fraction on the volume drop size distribution for 339 mPa · s silicone oil emulsions, at a flow rate of 300 kg/h and rotor speed of 11,000 rpm.

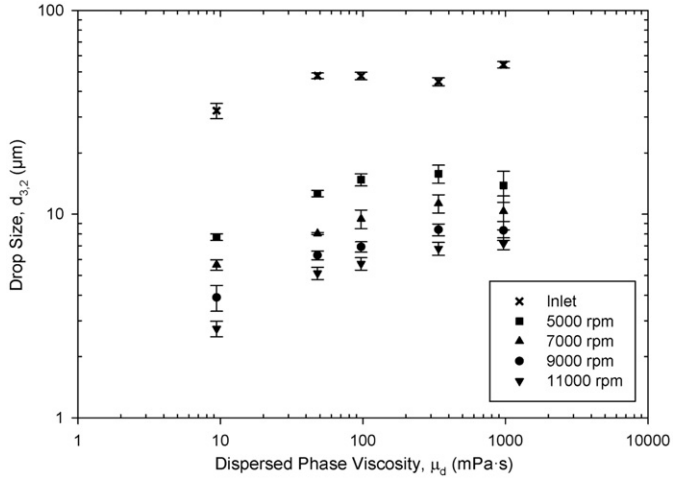

Fig. 10. Effect of dispersed phase viscosity on drop size for a range of rotor speeds for a flow rate of 300 kg/h and dispersed phase fraction of 1 wt.%. The inlet drop sizes range from 28 to 54 μm.

speed of 13.2 m/s, the changes in drop size was minimal. This value is close to the tip speed of the Silverson 150/250 at 4000 rpm (U_T=13.3 m/s); thus, their finding is consistent with rotor–stator mixers.

3.5. The effect of dispersed phase viscosity on droplet size

Fig. 10 shows the effect of dispersed phase viscosity on droplet size for a range of rotor speeds, and shows Sauter mean diameter to gradually increase with dispersed phase viscosity before it begins to plateau. This plot also clearly supports the differences in the trends observed for 9.4 mPa s oil in Figs. 4 and 6. Padron (2005) found a similar effect for a surfactant free emulsion in a batch Silverson where drop size increased with μ_d for 9.4–969 mPa s, followed by a constant droplet size. He suggested that the plateau was reached due to a shift towards an extensional flow breakage mechanism, which favours the breakage of the high viscosity droplets. This mechanism slowly deforms highly viscous drops by stretching them into long threads that break down over time resulting in the formation of two daughter drops with a number of smaller satellite drops. As oil viscosity increases, drop stability rises creating longer threads prior to break-up (Janssen and Meijer, 1993), and the production of a larger population of smaller satellite drops during extensional breakage, which accounts for the bimodal distribution seen in Fig. 5 for the highest viscosity oils.

In Fig. 10 for the lower rotor speeds, it may be seen that the drop size decreases slightly at the highest oil viscosity, which was also observed by Padron (2005) and is likely to result from the shift in breakage mechanism. Higher oil viscosities will stretch more under the applied velocity gradients, which results in a larger population of smaller droplets, increased bimodality and a reduced mean droplet size. However the standard deviation error bars for the high viscosity data are large and overlap for different rotor speeds, which is due in part to the bimodality of the distribution as it is harder to measure a wide range of droplets accurately by the same measuring technique. In addition, Sauter mean diameter is not an ideal parameter for describing bimodal size distributions.

Fig. 11 shows the effect of viscosity on the cumulative volume distributions at 11,000 rpm. The plot shows the previously discussed shift in droplet size to larger sizes with dispersed phase viscosity, and indicates that the volume distribution for the 9.4 mPa s oil is more distinct from the other viscosities. In terms of volume, both 9.4 and 97 mPa s distributions are similar in shape as they are both monomodal and more log-normally distributed, while the 969 mPa s oil curve bends more at larger drop sizes as the distribution is bimodal with a higher proportion of larger sized droplets. The highest oil viscosity distribution also forms a significantly larger maximum droplet size of ~70 μm; however, the smallest droplet sizes for all oil viscosities are close at 1–2 μm.

The volume DSDs (Fig. 5) are log-normal as observed by Padron (2005) for a batch Silverson. This differs from stirred tanks where normal or Gaussian distributions are formed for low μ_d systems, and log-normal distributions for high μ_d (Wang and Calabrese, 1986). Calabrese et al. (1986) examined silicone oil emulsions in stirred tanks and established that the drop size distribution broadened as μ_d increases, with the size of the largest and smallest drops both increasing and decreasing, respectively. This study found the size of the largest drop to rise with μ_d, but the size of the smallest drop did not decrease as viscosity increased (Fig. 11).

Arai et al. (1977) found drop size to remain constant when plotted against viscosity for $\mu_d < 10$ mPa s. Drop size then

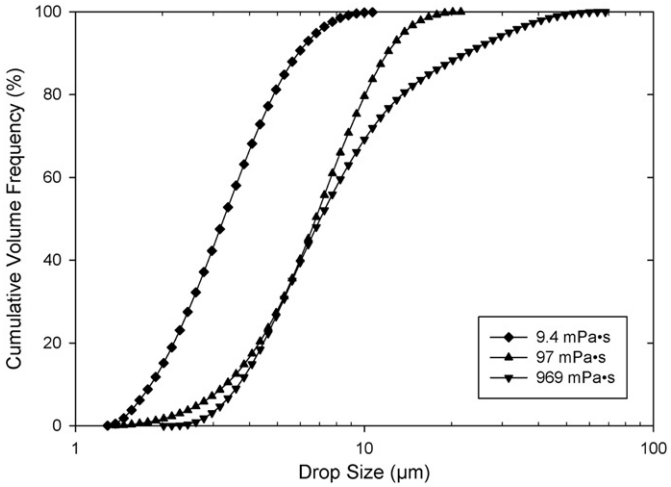

Fig. 11. Effect of dispersed phase viscosity on the cumulative volume drop size distributions for 1 wt.% emulsions of 9.4 mPa · s, 97 mPa · s and 969 mPa · s silicone oils at a rotor speed of 11,000 rpm and flow rate of 300 kg/h.

increased until a gradient of −0.75 was reached for μ_d > 200 mPa s, as given by Eq. (4). However, for μ_d > 1500 mPa s, the slope begins to level off with increases in viscosity, as is the case for this study for higher oil viscosities. It was stated that a possible reason for this observation at high μ_d could be as a result of more viscous droplets taking a longer time to return to a spherical shape between turbulent fluctuation time intervals. Hence, subsequent turbulent fluctuations will act upon a drop which becomes steadily more deformed and more prone to forming smaller drops (Arai et al., 1977). Wang and Calabrese (1986) examined silicone oil viscosities of 1 to 1000 mPa s, dispersed in water using a Rushton turbine and obtained a plot similar to Arai et al. (1977) where the relationship between drop size and dispersed phase viscosity is constant < 10 mPa s, rising to a gradient of 0.75, before levelling off at 1000 mPa s. Ludwig et al. (1997) investigated viscosities of 32 to 190 mPa s for a flow rate of 50 l/h and produced similar results to Arai et al. (1977), but with an increase in drop size above 50 mPa s and a plateau at ~200 mPa s.

The data from this study is consistent with previous work in that drop size increases as viscosity increases, but above a critical value of viscosity, drop size tends to become independent of the dispersed phase viscosity. If the Sauter mean diameter is correlated with either of the drop size correlations which account for the effect of dispersed phase viscosity, Eqs. (5) and (6), neither expression provides a good correlation. The reason for this may be because these correlations are based on the Kolmogorov theory assuming homogenous isotropic turbulence, and droplet breakage is likely to occur by a combination of breakage mechanisms.

The span of the drop size distribution provides information about the spread of the data values. Span is a measurement of the width of the distribution and is defined by

$$span = \frac{d_{0.9} - d_{0.1}}{d_{0.5}} \tag{10}$$

Span was found not to correlate strongly with the rotor speed, flow rate and dispersed phase fraction, however μ_d does influence span significantly. The span increases linearly with dispersed phase viscosity, and is well correlated with an R^2 of 0.949. At 9.4 mPa s the span averaged at 1.08 over a range of rotor speeds, rising to 3.18 at 969 mPa s. A broadening of the drop size distribution was also found by Ludwig et al. (1997) for increasing μ_d. The width of the distribution increases greatly as the size of the largest droplet increases and there is also a growing formation of smaller droplets seen with increasing oil viscosity (Fig. 11).

3.6. The effect of viscosity ratio on droplet size

Fig. 12 shows the effect of the continuous phase viscosity on droplet size. This plot indicates that decreasing the viscosity ratio reduces the droplet size for all viscosities examined, except for the lowest oil viscosity of 9.4 mPa s where the drop size increases then decreases again. The result for the higher oil viscosities is expected since a more viscous continuous phase can transmit the shear stress to the droplet interface more effectively, however the result for the 9.4 mPa s oil is unforeseen. The drop size curves for this oil viscosity appear to go through a maximum around a continuous phase viscosity of ~5 mPa s.

For nearly all the cases when the continuous phase is thickened, the Kolmogorov length scale increases so that all the droplets formed are below η_K (Table 3). For drops below η_K, Shinnar's (1961) model in Eq. (2) for the viscous subrange where inertial stress are important gives an exponent on μ_c of 0.33, and Eq. (3) for viscous stress gives −0.5. The results in Fig. 12 suggests that for viscosities of 48–969 mPa s, viscous stresses are more important for droplet breakage. For the

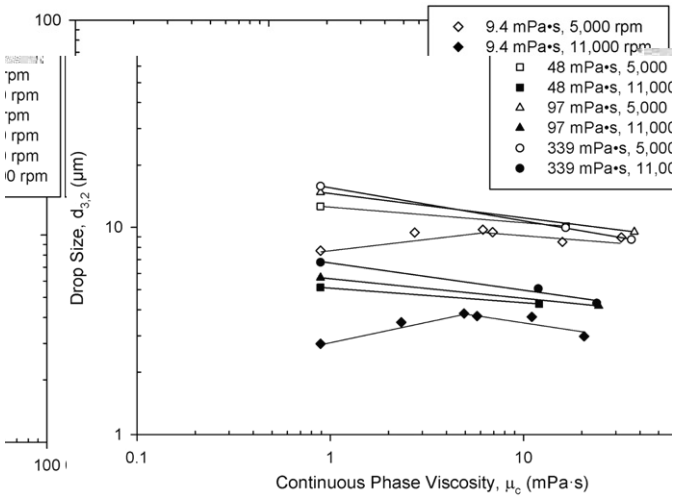

Fig. 12. Effect of continuous phase viscosity on drop size for a range of dispersed phase viscosities at rotor speeds of 5000 rpm and 11,000 rpm, for a flow rate of 300 kg/h and dispersed phase fraction of 1 wt.%.

Fig. 13. Dimensionless drop size as a function of the correlation presented by Equation 11, for a flow rate of 300 kg/h and dispersed phase fraction of 1 wt.%.

9.4 mPa s oil there appears to be a transition from where inertial stresses are dominant, to where viscous stresses play a greater role in droplet breakage. The importance of both inertial stresses for drops above η_K and viscous stresses for drops below η_K was also concluded by Calabrese et al. (2000) for a batch rotor-stator mixer. However, the exponents on μ_c in Eqs. (2)–(3) for the data in Fig. 12 are both less steep than indicated by the models which suggests that neither model can exclusively describe droplet breakage.

For a constant *Po*, Eq. (1) can be simplified to the following form to correlate droplet size using Weber number, and modified by adding viscosity ratio

$$\frac{d_{3.2}}{D} = 0.201\left(\frac{\mu_d}{\mu_c}\right)^{0.066} We^{-0.6} \tag{11}$$

This expression gives a power law fit to the data with R^2=0.971 for all droplet sizes formed where drop size decreases with increasing viscosity ratio, where drop breakage is dominated by viscous stresses (Fig. 13). This reasonable correlation indicates that for droplets primarily broken by viscous stresses, the effect of viscosity ratio on droplet size is relatively weak, which was also

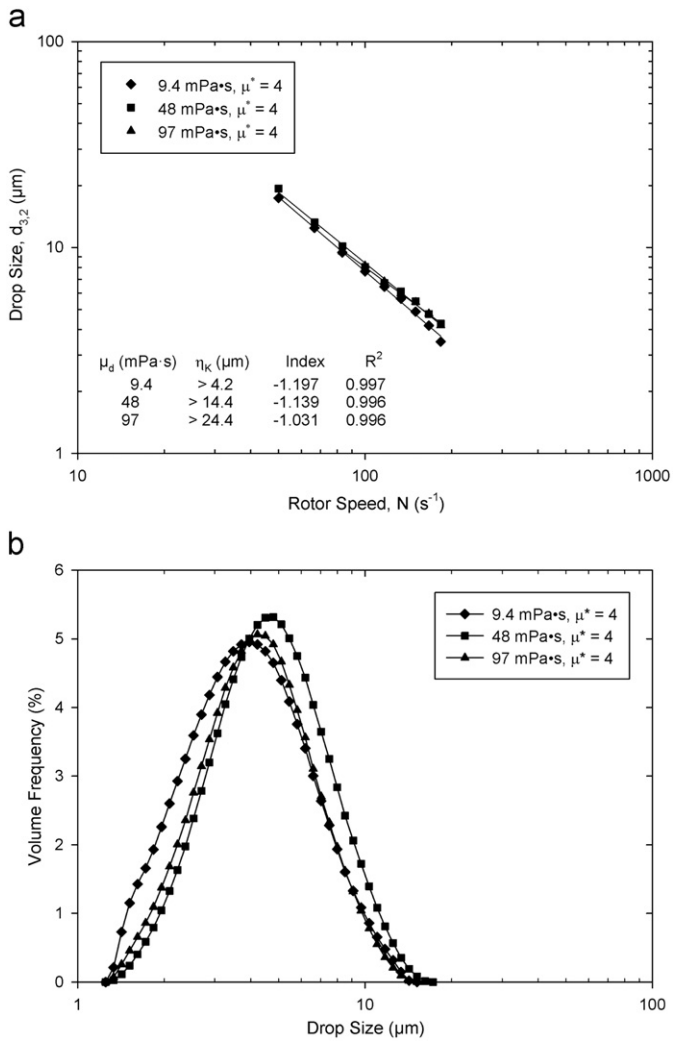

Fig. 14. (a) The effect of rotor speed on drop size for selected 1 wt.% silicone oil emulsions at a constant viscosity ratio of 4.0, for a flow rate of 300 kg/h, and (b) the effect of dispersed phase viscosity on the volume drop size distribution for 1 wt.% silicone oil emulsion at a constant viscosity ratio of 4.0. Flow rate is 300 kg/h and rotor speed is 11,000 rpm.

found by Calabrese et al. (2002) for a batch rotor–stator using glycerol solutions.

It may be observed from a plot (Fig. 14a) of drop size with rotor speed for viscosities of 9.4–97 mPa·s oil, at a constant viscosity ratio of 4.0, that the gradient reduces in magnitude from −1.20 to −1.03 as dispersed phase viscosity increases. Similar trends are found with energy dissipation rate as the increase in continuous phase viscosity was found to have a negligible impact upon the power draw which was measured for each experiment. The exponent on N for viscous stress in Eq. (3) is −1.5, therefore the reduction in the exponent with increasing μ_c suggests that drops are still broken by a combination of inertial and viscous stresses as the exponents are between −1 and −1.5.

Therefore, the experimental data does not follow all of the energy dissipation rate trends described by the theoretical models in Eqs. (1)–(3) for increasing μ_c. The drop size analysis technique is restricted to a minimum droplet size of 1.2 μm, hence droplets smaller than this are not measured (Fig. 14b) and will result in the gradients to become less steep. In addition, the Reynolds number (Re) for the highest continuous phase viscosity is ∼10,000, which from the power curve for the in-line Silverson 150/250 MS is at the point where the flow becomes transitional (Cooke et al., in press). The theoretical models are developed for turbulent flows, thus at larger continuous phase viscosities the models may not accurately describe the trends in droplet size reduction (Fig. 14a) as transitional flow, and in some areas of the mixing head where the flow has little time to develop, laminar flow breakage may begin to have an impact on droplet break-up.

Ludwig et al. (1997) also found drop size to reduce when continuous phase viscosity was increased from 1 to 200 mPa s. Drop size remained roughly constant up to a viscosity of around 10 mPa s, before decreasing as μ_c is reduced further. Khopkar et al. (2009) also found droplet size to decrease with viscosity ratio for a given energy density.

In general, the drop size distribution broadens for decreases in viscosity ratio. For a dispersed phase viscosity of 97 mPa·s (μ^*=109), the span averaged at 1.39 over a range of N, while for a μ^* of 4.0, span increased slightly to 1.95. This finding is consistent with results by Noro (1978) for emulsions in stirred vessels, who also obtained broadening drop size distributions with decreasing viscosity ratio.

Vankova et al. (2007) examined the effect of continuous phase viscosity on a 1% 95 mPa s silicone oil emulsion, using glycerol to create a range of continuous phase viscosities up to ∼18 mPa s. Vankova et al. (2007) found a three-fold reduction of drop size over the viscosity ratio range of 95–5.3, compared to a reduction from 5.7 to 4.2 μm for a similar range of μ^* in this investigation, and they concluded that the droplet breakage mechanism changed as the regime transformed from turbulent inertial to turbulent viscous.

3.7. Energy dissipation rate and energy density

Fig. 15 presents two commonly used parameters for scale-up, namely energy dissipation rate based on the swept volume of the rotor for high shear mixers, and energy density. Both of these parameters are calculated from the power draw of the mixer which is obtained as described by Kowalski (2009) and Kowalski et al. (2011). Fig. 15a is very similar to Fig. 4 since at a fixed flow rate and a single mixer scale, power draw is entirely dependent on the rotor speed. The exponents of −0.39 to −0.45 for viscosities of 9.4–339 mPa s are close to the value of −0.48 found by Calabrese et al. (2000) for a batch Ross rotor–stator mixer. At the highest rotor speed of 11,000 rpm where a range flow rates were investigated, as the power draw increases there is a slight increase in drop size (Fig. 6). However, energy dissipation rate is not sufficient to describe the behaviour for continuous processes; hence energy density is more appropriate as it accounts for mean residence time.

Fig. 15b presents drop size in terms of energy density. At a fixed flow rate (M=300 kg/h), increasing the rotor speed (closed symbols) increases the amount of energy used per unit volume of fluid, and smaller drop sizes are formed as expected. The exponents are −0.45 and −0.39 for 9.4 and 48–969 mPa s oil respectively, which are similar to those obtained for turbulent inertial forces for rotor–stator systems when b is −0.4 (Karbstein and Schubert, 1995). At a fixed rotor speed (N=11,000 rpm), increasing the flow rate (open symbols) has a much weaker effect on drop size as seen in Fig. 6, and the exponents on energy density are 0.24 and 0.04 for 9.4 and 48–969 mPa s oil respectively. As a result, Fig. 15b indicates that at a constant rotor speed, the higher flow rates have the lowest energy density since total power draw is a weak function of flow rate (Kowalski et al., 2011). Thus, increasing the flow rate at a constant rotor speed will increase the power drawn, but this increase is marginal compared to the additional fluid processed, which overall reduces energy density. Consequently, to obtain a given droplet size it is much more

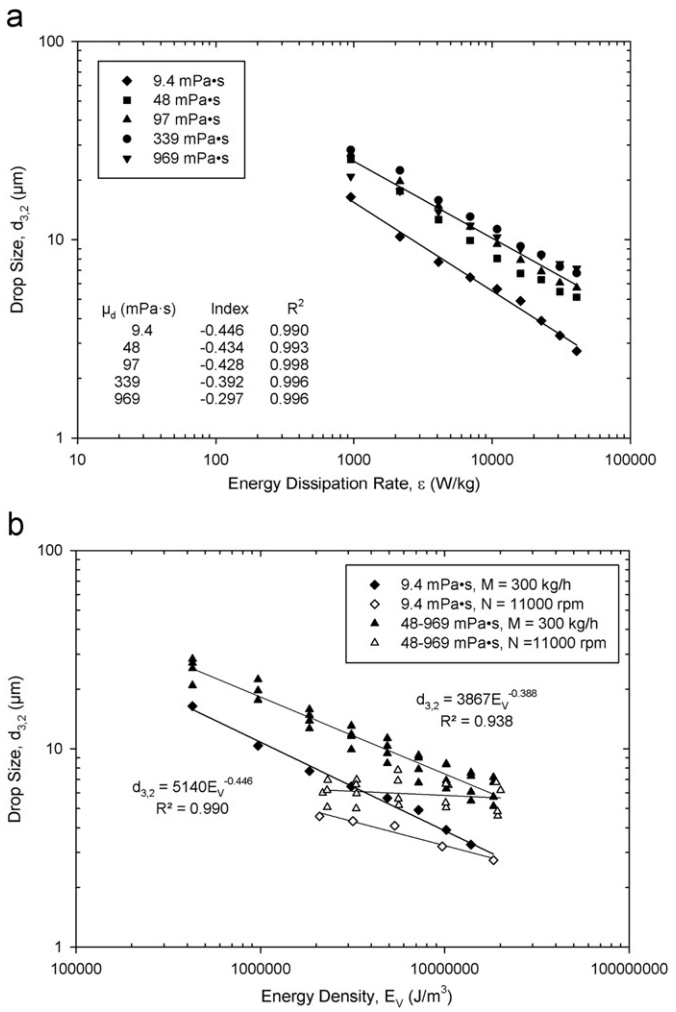

Fig. 15. Drop size presented as a function of (a) energy dissipation rate and (b) energy density for a range of dispersed phase viscosities. In (b), closed symbols are a constant flow rate of 300 kg/h and rotor speeds of 3000–11,000 rpm. Open symbols are a constant rotor speed of 11,000 rpm and flow rates of 300–4800 kg/h. Dispersed phase fraction is 1 wt.%.

energy efficient to operate the mixer at as high a flow rate as possible. Increasing the flow rate is efficient as more of the pumping capability of the Silverson is utilised, as restricting the flow rate results in energy wastage through generation of large pressure gradients, and increased outlet temperatures at reduced residence times.

4. Conclusions

Droplet break-up by an in-line Silverson high shear rotor–stator mixer has been investigated, and the droplet size has been correlated against theoretical models based on energy dissipation rate and the commonly used scale-up term of energy density. Drop size correlations with energy density indicate that to obtain a given droplet size it is more energy efficient to operate the mixer at as high flow rate as possible.

Emulsion droplet size is primarily influenced by the effect of the rotor speed, and was found to be almost independent of flow rate, especially for higher oil viscosities, and produced droplets as small as 2–3 μm after a single pass. The inlet droplet size ranged from 23 to 62 μm and was found not to greatly affect the outlet droplet size. Similarly the dispersed phase volume fraction was found not to affect the droplet size significantly for the range studied of 1–50 wt%, due to the presence of excess surfactant. Thus it may be concluded that the droplet size produced by the Silverson is largely a function of rotor speed and there is little advantage of improving the emulsification efficiency of earlier stages in the process, such as dispersion in stirred vessels.

Droplet size increases as dispersed phase viscosity increases, but begins to reach a plateau at a viscosity of 97 mPa s and is constant at around 969 mPa s. At the highest viscosity, the volume drop size distributions are bimodal which points to a change of breakage mechanism closer to pure extensional flow. The width of the distributions also broadens as the dispersed phase viscosity increases. For a constant dispersed phase viscosity, reducing the viscosity ratio improves droplet break-up as a consequence of improved transmission of stresses to the droplet surface. However for the lowest oil viscosity investigated the droplet size goes through a maximum as μ^* is increased.

The drop sizes obtained are of the same order of magnitude as the Kolmogorov length scale, thus droplet breakage is likely to occur by several mechanisms. Applying the well established theory based on Kolmogorov, the results indicate that low viscosity droplets larger than the Kolmogorov length scale are most likely broken by turbulent inertial stresses, while droplets smaller than the Kolmogorov length scale are broken by a combination of inertial and viscous stresses. The drop size distributions also suggest that high viscosity drops are broken by extensional flows forming bimodal distributions. However, the drop size data does not follow all of the trends described by the theoretical models, but the models are based on the theory of Kolmogorov which assumes homogenous isotropic turbulence which is unlikely to be present in the mixing head.

It has not been possible to easily distinguish between various breakage mechanisms and scale-up approaches, therefore further studies will investigate the effect of scale, physical properties of the emulsion and the number of passes through the mixer on droplet size.

Nomenclature

Symbols

b	exponent (dimensionless)
C, $C_1 \ldots C_6$	empirical constants (dimensionless)
D	outer rotor diameter (m)
$d_{3,2}$	surface area weighted mean drop diameter (Sauter mean drop diameter) (m)
$d_{4,3}$	mass mean drop diameter (m)
$d_{1,0}$, $d_{5,0}$, $d_{9,0}$	drop diameters defined by cumulative volume frequencies (m)
$E_v = P/Q$	energy density (J/m^3)
k	constant (Pa s)^n
M	mass flow rate (kg/s)
N	rotor speed (s^{-1})
n	power law index (dimensionless)
P	power (W)
Q	volumetric flow rate (m^3/s)
R^2	linear regression correlation coefficient (dimensionless)
U_T	tip speed (m/s)
V_H	volume of mixing head (m^3)

Greek symbols

$\dot{\gamma}$	shear rate (s^{-1})
$\varepsilon = P/\rho_c V_H$	energy dissipation rate per unit mass of fluid (W/kg)
$\eta = k\dot{\gamma}^{n-1}$	apparent viscosity of continuous phase (Pa s)

$\eta_K = (v_c{}^3/\varepsilon)^{1/4}$ Kolmogorov length scale of turbulence (m)
μ_c continuous phase viscosity (Pa s)
μ_d dispersed phase viscosity (Pa s)
$\mu* = \mu_d/\mu_c$ viscosity ratio (dimensionless)
$v_c = \mu_c/\rho_c$ kinematic viscosity of continuous phase (m^2/s)
ρ_c continuous phase density (kg/m^3)
ρ_d dispersed phase density (kg/m^3)
σ interfacial tension (N/m)
Φ dispersed phase volume fraction (dimensionless)

Dimensionless groups

$Po = P/\rho_c N^3 D^5$ power number (dimensionless)
$\mathrm{Re} = \rho_c ND^2/\mu_c$ Reynolds number (dimensionless)
$Vi = (\rho_c/\rho_d)^{1/2}\mu_d ND/\sigma$ viscosity group (dimensionless)
$We = \rho_c N^2 D^3/\sigma$ Weber number (dimensionless)

Acknowledgements

The authors would like to acknowledge the Engineering and Physical Sciences Research Council (ESPRC) and Unilever for EngD funding, and the Royal Commission for the Exhibition of 1851 for the Industrial Fellowship for S. Hall, the Royal Society of the UK for the Industry Fellowship for A.J. Kowalski, and the support by a further research grant from Unilever for A. El-Hamouz and M. Cooke. S. Hall would also like to acknowledge Lucie Gangolf, Guillaume Munsch, Mylène Parriaud and Clément Vannier of The University of Manchester/Nancy-Université INPL for help and support with experimental work and analysis, Prof. Andrzej Pacek for advice and suggestions on compiling this article, and The University of Manchester's School of Chemical and Analytical Science workshop staff for help with modifications and maintenance of the equipment.

References

Adler-Nissen, J., Mason, S.L., Jacobsen, C., 2004. Apparatus for emulsion production in small scale and under controlled shear conditions. Trans. IChemE, Part C, Food Bioproducts Process. 82 (C4), 311–319.
Arai, K., Konno, M., Matunaga, Y., Saito, S., 1977. Effect of dispersed-phase viscosity on the maximum stable drop size for breakup in turbulent flow. J. Chem. Eng. Japan 10, 325–330.
Atiemo-Obeng, V.A., Calabrese, R.V., 2004. Rotor–stator mixing devices. In: Paul, E.L., Atiemo-Obeng, V.A., Kresta, S.M. (Eds.), Handbook of Industrial Mixing. John Wiley & Sons, Inc. Chapter 8.
Averbukh, Yu.N., Nikoforov, A.O., Kostin, N.M., Korshakov, A.V., 1988. Computation of dispersion for emulsions formed in a rotor–stator unit. Journal of Applied Chemistry of the USSR 61 (2), 396–397.
Calabrese, R.V., Francis, M.K., Kevala, K.R., Mishra, V.P., Padron, G.A., Phongikaroon, S., 2002. Fluid dynamics and emulsification in high shear mixers, in: Proc. 3rd World Congress on Emulsions. Lyon, France.
Calabrese, R.V., Francis, M.K., Kevala, K.R., Mishra, V.P., Phongikaroon, S., 2000. Measurement and analysis of drop size in a batch rotor–stator mixer, in: Van den Akker, H.E.A., Derksen, J.J., (Eds.), 10th European Conference on Mixing. Elsevier Science, Amsterdam, pp. 149–156.
Calabrese, R.V., Chang, T.P.K., Dang, P.T., 1986. Drop breakup in turbulent stirred-tank contactors Part I: effect of dispersed-phase viscosity. AIChE J. 32 (4), 657–666.
Cooke, M., Rodgers, T., Kowalski, A.J. Power characterisation of an in-line Silverson high shear mixer. AIChE J, in press, AIChE-10-12800.R2.
Davies, J.T., 1985. Drop sizes of emulsions related to turbulent energy dissipation rates. Chem. Eng. Sci. 40 (5), 839–842.
Davies, J.T., Rideal, E.K., 1961. Interfacial Phenomena. Academic Press, New York.
El-Hamouz, A., Cooke, M., Kowalski, A., Sharratt, P., 2009. Dispersion of silicone oil in water surfactant solution: effect of impeller speed, oil viscosity and addition point on drop size distribution. Chem. Eng. Process. 42 (2), 633–642.
El-Hamouz, A., 2007. Effect of surfactant concentration and operating temperature on the drop size distribution of silicon oil water dispersion. J Disper. Sci. Technol. 28 (5), 797–804.
Gingras, J.-P., Tanguy, P.A., Mariotti, S., Chaverot, P., 2005. Effect of process parameters on bitumen emulsions. Chem. Eng. Process. 44, 979–986.
Goloub, T., Pugh, R.J., 2003. The role of the surfactant head group in the emulsification process: single surfactant systems. J. Colloid Interface Sci. 257, 337–343.
Hinze, J.O., 1955. Fundamentals of the hydrodynamic mechanism of splitting in dispersion processes. AIChE J. 1 (3), 289–295.
Janssen, J.M.H., Meijer, H.E.H., 1993. Droplet breakup mechanisms—stepwise equilibrium versus transient dispersion. J. Rheol. 37 (4), 597–608.
Karbstein, H., Schubert, H., 1995. Developments in the continuous mechanical production of oil-in-water macro-emulsions. Chem. Eng. Process. 34, 205–211.
Kevala, K.R., Kiger, K.T., Calabrese, R.V., 2005. Single pass drop size distributions in an inline rotor–stator mixer. APS Division of Fluid Dynamics 58th Annual Meeting (DFD05), Chicago, IL. Paper No. GB.00004.
Khopkar, A.R., Fradette, L., Tanguy, P.A., 2009. Emulsification capability of a duel shaft mixer. Chem. Eng. Res. Des. 87, 1631–1639.
Kowalski, A.J., Cooke, M., Hall, S., 2011. Expression for turbulent power draw of an in-line Silverson high shear mixer. Chem. Eng. Sci. 66, 241–249.
Kowalski, A.J., 2009. An expression for the power consumption of in-line rotor–stator devices. Chem. Eng. Process. 48, 581–585.
Leng, D.E., Calabrese, R.V., 2004. Immiscible liquid–liquid systems. In: Paul, E.L., Atiemo-Obeng, V.A., Kresta, S.M. (Eds.), Handbook of Industrial Mixing. John Wiley & Sons, Inc. Chapter 12.
Ludwig, A., Flechtner, U., Pruss, J., Warnecke, H.-J., 1997. Formation of emulsions in a screw loop reactor. Chem. Eng. Technol. 20, 149–161.
Maa, Y.-F., Hsu, C., 1996. Liquid–liquid emulsification by rotor/stator homogenization. J. Controlled Release 38, 219–228.
Myers, K.J., Reeder, M.F., Ryan, D., Daly, G., 1999. Get a fix on high-shear mixing. Chem. Eng. Prog. 95, 33–42.
Noro, S., 1978. Studies on liquid–liquid dispersion by mechanical agitation. Prog. Org. Coat. 6, 271.
Pacek, A.W., Chamsart, S., Nienow, A.W., Bakker, A., 1999. The influence of impeller type on mean drop size and drop size distribution in an agitated vessel. Chem. Eng. Sci. 54, 4211–4222.
Padron, G.A., 2005. Effect of surfactants on drop size distribution in a batch, rotor–stator mixer. PhD Thesis, University of Maryland, MD, USA.
Saadevandi, B.A., Zakin, J.L., 1996. A study of silicone oil-in-water emulsions. Chem. Eng. Commun. 156, 227–246.
Schubert, H., Engel, R., 2004. Product and formulation engineering of emulsions. Trans IChemE, Part A, Chem. Eng. Res. Des. 82 (A9), 1137–1143.
Schubert, H., 1997. Advances in the mechanical production of food emulsions, in: Proceedings of the 7th International Congress on Engineering and Food. Part 1, S. pp. 82–87.
Shinnar, R., 1961. On the behaviour of liquid dispersions in mixing vessels. J. Fluid Mech. 10, 259–275.
Thapar, N., 2004. Liquid–liquid dispersions from in-line rotor–stator mixers. PhD Thesis, Cranfield University, UK.
Utomo, A.T., Baker, M., Pacek, A.W., 2009. The effect of stator geometry on the flow pattern and energy dissipation rate in a rotor–stator mixer. Chem. Eng. Res. Des. 87, 533–542.
Vankova, N., Tcholakova, S., Denkov, N.D., Ivanov, I.B., Vulchev, V.D., Danner, T., 2007. Emulsification in turbulent flow: 1. Mean and maximum drop diameters in inertial and viscous regimes. J. Colloid Interface Sci. 312, 363–380.
Wang, C.Y., Calabrese, R.V., 1986. Drop breakup in turbulent stirred-tank contactors: part II: relative influence of viscosity and interfacial tension. AIChE J. 32 (4), 667–676.